

# Dineutron structure in $^8\text{He}$

Yoshiko Kanada-En'yo

Yukawa Institute for Theoretical Physics, Kyoto University, Kyoto, Japan

The ground and excited states of  $^8\text{He}$  were investigated with a method of antisymmetrized molecular dynamics(AMD). We adopted effective nuclear interactions which systematically reproduce the binding energies of  $^4\text{He}$ ,  $^6\text{He}$  and  $^8\text{He}$ . The ground state of  $^8\text{He}$  has both the  $j$ - $j$  coupling feature( $p_{3/2}$  closure) and the  $L$ - $S$  coupling feature( $^4\text{He}+2n+2n$ ) with a slight tail of dineutron at the long distance region. The theoretical results give an indication of the  $0_2^+$  state with dineutron gas-like structure. The dineutron structure,  $^4\text{He}+2n+2n$ , of this state is similar to the  $3\alpha$ -cluster structure of the  $^{12}\text{C}(0_2^+)$  state which has been interpreted as an  $\alpha$  condensate state. Since the  $^8\text{He}(0_2^+)$  state has a significant overlap with the dineutron condensate wave function where two dineutrons are moving in  $S$  wave around the  $\alpha$  core with a dilute density, we suggest that this theoretically predicted  $0_2^+$  state is a candidate of the dineutron condensate state.

## I. INTRODUCTION

In the recent progress of unstable nuclear physics, various kinds of exotic structure have been discovered. Many of these phenomena in light nuclear region are often related to cluster physics. From the viewpoints of nuclear cluster, there are many theoretical works on halo structure in neutron-rich nuclei and molecular structure in Be isotopes. Recently, Tohsaki *et al.* proposed a new type of cluster structure in the second  $0^+$  state  $^{12}\text{C}$ , where 3  $\alpha$  clusters are weakly interacting[1]. This is a dilute gas state of  $\alpha$  particles which behave as bosonic particles in the dilute density. This phenomena is associated with Bose-Einstein Condensation(BEC) and is called “alpha condensation”. The alpha condensation was originally suggested in dilute nuclear matter by Röpke et al.[2]. The  $0_2^+$  of  $^{12}\text{C}$  is regarded as an example, where the alpha condensation is realized in a finite nuclear system. Then, it is challenging to search for such cluster-gas states in other nuclei. In analogy to the alpha condensation, dineutron condensation in neutron matter is a recent key issue in physics of unstable nuclei. Matsuo suggested that the dineutron correlation can be enhanced in dilute neutron matter[3]. In real systems, one should focus on dineutron correlation in finite nuclei such as halo nuclei and extremely neutron-rich nuclei, or that in neutron skin at a surface region of neutron-rich nuclei. In fact, the dineutron correlation in two-neutron halo nuclei like  $^6\text{He}$  and  $^{11}\text{Li}$  attracts great interests in these days. In case of  $^6\text{He}$ , where the  $^4\text{He}$  is the good core, the dineutron correlation of the valence neutrons has been demonstrated in three-body model calculations (for example, [4, 5, 6, 7] and references therein).

Now, let us consider structure of  $^8\text{He}$  from a point of view associated with the dineutron condensation. Firstly, more than one dineutrons are required to construct a dineutron condensate state. In  $^8\text{He}$ , two pairs of neutrons are possible from four valence neutrons around the  $^4\text{He}$  core. In second,  $^8\text{He}$  system may have some correspondence with the  $^{12}\text{C}$  system, because both of them have the same neutron number,  $N = 6$ . In analogy to  $^{12}\text{C}$ , the ground state of  $^8\text{He}$  may have a feature of the neutron  $p_{3/2}$  closure or the  $\text{SU}(3)$ -limit  $p$ -shell configuration. Instead of the ground state, one can speculate the dineutron gas-like state with developed  $^4\text{He}+2n+2n$  structure in excited states.

There are many theoretical works on He isotopes. Application of *ab initio* calculations such as GFMC and NCSM with realistic nuclear forces have now reached to the mass  $A \sim 10$  region including  $^6\text{He}$  and  $^8\text{He}$ [8, 9, 10]. Systematic studies of He isotopes have been performed also by model calculations with effective interactions such as cluster models as well as GSM[11, 12, 13] and mean field approaches[14]. Three-body model with an assumption of the  $^4\text{He}$  core has been often adopted to study  $^6\text{He}$  [4, 5, 6, 7, 15, 16] and it has been applied to heavier He isotopes [17].  $^8\text{He}$  and  $^{10}\text{He}$  have been also studied by such models as  $^4\text{He}+Xn$  models [18, 19, 20, 21] and by extended models [22, 23] which have less assumption of the core. With Fermionic molecular dynamics, the study of He isotopes has been performed based on a realistic nuclear force [24]. However, many of these studies are concentrated on the ground states except for three-body models, GSM and GFMC.

After the experimental indication of neutron skin structure in  $^8\text{He}$ [25], many experimental works on  $^8\text{He}$  have been recently performed to reveal the detailed properties of the ground state. The core excitation  $^6\text{He}(2^+)$  in the ground state, which has been experimentally suggested[26], indicates that  $^8\text{He}$  is different from a simple three-body state of  $^6\text{He}(0^+)+2n$ . Recent experiments using  $^8\text{He}$  beams suggested the significant component of the  $(p_{3/2})^2(p_{1/2})^2$  configuration [27, 28]. They may support dineutron correlation in the  $^8\text{He}$  ground state rather than the pure  $(p_{3/2})$  closure of neutrons. On the other hand, a measurement of spectroscopic factor of  $^7\text{He}(3/2^-)$ [29] in  $^8\text{He}$  suggested the pure sub-shell closed structure contradictory to the other experimental results. Thus, the neutron structure of the  $^8\text{He}$  ground state is controversial. Concerning excited states, although some levels are known to exist in the energy

$E_x = 3 \sim 8$  MeV region, the experimental information is very poor for these states except for the  $2_1^+$  state [30].

In this paper, we investigated structure of  $^8\text{He}$ . In particular, we focused on  $0^+$  states and discuss their dineutron component, because one of our major aims is to search for the dineutron gas-like state. We applied a method of antisymmetrized molecular dynamics(AMD)[31, 32, 33], which has been already proved to be useful in describing cluster structure in light nuclei. AMD has been applied to various light unstable nuclei such as He, Li, Be isotopes as well as stable nuclei. It has been applied also for study of cluster gas-like states in  $^{12}\text{C}$  and  $^{11}\text{C}(^{11}\text{B})$ [34, 35]. In the present work, we adopted a AMD+generator coordinate method(GCM). Namely, we superposed a number of AMD wave functions, which were obtained by energy variation with constraints, to take various configurations into account. We comment that the theoretical method AMD+GCM of the present calculation is similar to those of the AMD+GCM and AMD+SSS works on He isotopes by Itagaki and his collaborators [20, 23] in a sense that multi configurations of AMD wave functions are superposed. In [20, 23],  $^4\text{He}+Xn$  and  $t+t+Xn$  configurations were *a priori* assumed. Another claim is that they used an effective interaction which makes a bound  $^2n$ . In the present work, we have no assumption of the cluster core and chose effective interactions by taking care of subsystem energies such as  $\alpha$ -n and  $^6\text{He}$  as well as nucleon-nucleon scattering. We used some sets of interaction parameters and showed the calculated results of the ground and excited states of He isotopes. By assuming  $(0s)^2$  configuration as the interior structure of a dineutron, we analyzed dineutron structure of  $^8\text{He}$  and compared it with the  $\alpha$ -cluster structure of  $^{12}\text{C}$ .

The paper is organized as follows. In the next section, we briefly explain the theoretical method of the present work. Results are given in III, and dineutron structure is discussed in IV. Finally, we give a summary in V.

## II. FORMULATION

In this section, we briefly explain the formulation of AMD+GCM in the present calculation. The detailed formulation of the AMD method for nuclear structure study is described in [32, 33]. There are various versions of practical methods of the AMD framework. In the present work, we performed superposition of a number of AMD wave functions obtained by energy variation with constraints based on the concept of GCM. The procedure of the variation, spin and parity projection and superposition is similar to those of AMD+GCM calculations in [20, 36, 37], though the details of model wave functions and effective interactions are different from each other.

An AMD wave function is a Slater determinant of Gaussian wave packets;

$$\Phi_{\text{AMD}}(\mathbf{Z}) = \frac{1}{\sqrt{A!}} \mathcal{A}\{\varphi_1, \varphi_2, \dots, \varphi_A\}, \quad (1)$$

where the  $i$ th single-particle wave function is written by a product of spatial( $\phi$ ), intrinsic spin( $\chi$ ) and isospin( $\tau$ ) wave functions as,

$$\varphi_i = \phi_{\mathbf{X}_i} \chi_i \tau_i, \quad (2)$$

$$\phi_{\mathbf{X}_i}(\mathbf{r}_j) = \left(\frac{2\nu}{\pi}\right)^{\frac{3}{4}} \exp\{-\nu(\mathbf{r}_j - \frac{\mathbf{X}_i}{\sqrt{\nu}})^2\}, \quad (3)$$

$$\chi_i = \left(\frac{1}{2} + \xi_i\right)\chi_{\uparrow} + \left(\frac{1}{2} - \xi_i\right)\chi_{\downarrow}. \quad (4)$$

$\phi_{\mathbf{X}_i}$  and  $\chi_i$  are spatial and spin functions, and  $\tau_i$  is isospin function which is fixed to be up(proton) or down(neutron). The width parameter  $\nu$  is chosen to be the optimum value for each system. Accordingly, an AMD wave function is expressed by a set of variational parameters,  $\mathbf{Z} \equiv \{\mathbf{X}_1, \mathbf{X}_2, \dots, \mathbf{X}_A, \xi_1, \xi_2, \dots, \xi_A\}$ .

The energy variation was performed for the parity-projected AMD wave function  $\Phi_{\text{AMD}}^{\pm}(\mathbf{Z})$  under constraints. In order to obtain basis wave functions, we adopted the total oscillator quanta and deformation as the constraints. Hereafter, we note the expectation value of an operator  $\hat{O}$  with respect to a normalized parity-projected AMD wave function as  $\langle \hat{O} \rangle$ . Expectation values  $\langle \hat{N}^{\text{ho}} \rangle$  of the total oscillator quanta is given by the creation and annihilation operators of harmonic oscillator in the same way as [37]. In the AMD+GCM calculations with the  $\beta$ -constraint (for example [36]), the deformation is usually constrained by using the rotational invariant value  $D \equiv \text{Tr}(QQ)/\text{Tr}^2(Q)$ , where the matrix  $Q$  is calculated by quadrupole operators as  $Q_{\sigma\rho} = \langle \sum_i \hat{\sigma}_i \hat{\rho}_i \rangle$  ( $\hat{\sigma} = \hat{x}, \hat{y}, \hat{z}$  and  $\hat{\rho} = \hat{x}, \hat{y}, \hat{z}$ ) [38]. Here  $D$  is approximately related to the quadrupole deformation parameter  $\beta$  as  $D(\beta) = (5\beta^2/2\pi + 1)/3$ . In the present work, we used the modified quadrupole matrix  $Q'_{\sigma\rho} \equiv Q_{\sigma\rho} - A\delta_{\sigma\rho}$  ( $A$  is the mass number) instead of the original  $Q_{\sigma\rho}$  and imposed the constraint on the  $D' \equiv \text{Tr}(Q'Q')/\text{Tr}^2(Q')$ . This is useful for He isotopes to obtain basis wave functions with various configurations on mesh points of the two-dimensional parameters,  $\beta$  and  $\langle \hat{N}^{\text{ho}} \rangle$ . The energy variation with the constraint values  $N_{\text{const}}$  and  $\beta_{\text{const}}$  was performed with respect to the parity-projected AMD wave function by minimizing the energy defined as,

$$E \equiv \langle \hat{H} \rangle + V^N (N_{\text{const}} - \langle \hat{N}^{\text{ho}} \rangle)^2 + V^{\beta} (D(\beta_{\text{const}}) - D')^2. \quad (5)$$

Here the artificial potentials are introduced to satisfy the condition of the constraints. With a given set of constraint values  $(N_{\text{const}}, \beta_{\text{const}})$  the optimum wave function  $\Phi_{\text{AMD}}^{\pm}(N_{\text{const}}, \beta_{\text{const}})$  was obtained. Finally, we superposed the spin-parity eigen states projected from the obtained wave functions,

$$|^8\text{He}(J_n^{\pm})\rangle = \sum_{N_{\text{const}}, \beta_{\text{const}}} c_n^{J^{\pm}}(N_{\text{const}}, \beta_{\text{const}}) |P_{MK}^J \Phi_{\text{AMD}}^{\pm}(N_{\text{const}}, \beta_{\text{const}})\rangle, \quad (6)$$

where the coefficients  $c_n^{J^{\pm}}(N_{\text{const}}, \beta_{\text{const}})$  were determined by diagonalizing the Hamiltonian and Norm matrices. In the present calculations, we took only  $M = K = 0$  states.

### III. RESULTS

#### A. Calculations

$^6\text{He}$ ,  $^8\text{He}$  and  $^{10}\text{He}$  were calculated by the AMD+GCM method. The strengths,  $V^N$  and  $V^{\beta}$ , for the constraint potentials in eq.5 are chosen to be 30 MeV and 2000 MeV, respectively. We chose the width parameter  $\nu$  to optimize the energy for the  $P_{(MK)=(00)}^{J=0} \Phi_{\text{AMD}}^+(N_{\text{const}} = N_{\text{min}} + 2)$ , which gives the minimum energy among the states  $P_{(MK)=(00)}^{J=0} \Phi_{\text{AMD}}^+(N_{\text{const}})$  in most cases. Here,  $N_{\text{min}}$  is the minimum value of the harmonic-oscillator quanta,  $N_{\text{min}} = 2, 4$ , and  $6$  for  $^6\text{He}$ ,  $^8\text{He}$ , and  $^{10}\text{He}$ , respectively. A common  $\nu$  value for each He isotope are used in the calculation with each interaction. The adopted  $\nu$  values are listed in table I. We adopted the constraint values of the mesh points  $(i, j)$  on the  $N_{\text{const}}\text{-}\beta_{\text{const}}$  plane as  $N_{\text{const}}^{(i)} = N_{\text{min}} + \Delta^{(i)}$  ( $\Delta^{(i)} = 0, 1, 2, 3, 4, 6, 8, 10$  for positive parity states and  $\Delta^{(i)} = 1, 2, 3, 4, 6, 8, 10$  for negative parity states) and  $\beta_{\text{const}}^{(j)} = 0, 0.2, 0.4, 0.6, \dots, 1.6$ . Then, the total number of the basis wave functions are 72(63) for positive(negative)-parity states. On the  $N_{\text{const}}\text{-}\beta_{\text{const}}$  plane, we first obtained the wave function  $\Phi_{\text{AMD}}^{\pm}(N_{\text{const}}, \beta_{\text{const}})$  at  $N_{\text{const}} = N_{\text{min}} + 2$  and  $\beta_{\text{const}} = 0, 0.2, 0.4, 0.6, \dots, 1.6$ . Then we searched for  $\Phi_{\text{AMD}}^{\pm}(N_{\text{const}} + 1, \beta_{\text{const}})$  (or  $\Phi_{\text{AMD}}^{\pm}(N_{\text{const}} - 1, \beta_{\text{const}})$ ) starting from the  $\Phi_{\text{AMD}}^{\pm}(N_{\text{const}}, \beta_{\text{const}})$  by increasing(or decreasing)  $N_{\text{const}}$  one by one.

Some of the basis wave functions with the constraints have the breaking of the  $^4\text{He}$ -core. Such the basis wave functions with the  $^4\text{He}$ -core breaking have high energies in general, and therefore, they practically give only small contribution to the low-lying states of  $^6\text{He}$ ,  $^8\text{He}$  and  $^{10}\text{He}$  isotopes. It means that the  $^4\text{He}$  cluster is a rather good core in  $^6\text{He}$ ,  $^8\text{He}$  and  $^{10}\text{He}$  isotopes, while the motion of valence neutrons is relatively important.

TABLE I: Parameter sets of the effective interaction and the values of width parameter  $\nu$  adopted in the present work. The theoretical values of scattering length  $a_s(a_t)$  for singlet(triplet) even channel, neutron separation energy of  $^5\text{He}$  ( $S_n(^5\text{He}) \equiv E(^4\text{He}) - E(^4\text{He-}n)$ ),  $2\alpha$  threshold energy of  $^8\text{Be}$ , two-neutron separation energies of  $^6\text{He}$  and  $^8\text{He}$  ( $S_{2n}(^6\text{He}) \equiv E(^4\text{He}) - E(^6\text{He})$ ) and  $S_{2n}(^8\text{He}) \equiv E(^6\text{He}) - E(^8\text{He})$ ) are also listed.

| Parameter set  |                     | v58         | v56         | m62         | m56         |
|--|---------------------|-------------|-------------|-------------|-------------|
| Central force  |                     | Volkov No.2 | Volkov No.2 | MV1 case(3) | MV1 case(3) |
| Wigner   | $w$                 | 0.42        | 0.44        | 0.38        | 0.44        |
| Bartlett   | $b$                 | 0           | 0.15        | 0           | 0.15        |
| Heisenberg   | $h$                 | 0           | 0.15        | 0           | 0.15        |
| Majorana   | $m$                 | 0.58        | 0.56        | 0.62        | 0.56        |
| $\nu(^4\text{He})$ (fm $^{-2}$ )                     |                     | 0.265       | 0.265       | 0.210       | 0.210       |
| $\nu(^6\text{He})$ (fm $^{-2}$ )                     |                     | 0.245       | 0.245       | 0.210       | 0.210       |
| $\nu(^8\text{He})$ (fm $^{-2}$ )                     |                     | 0.240       | 0.240       | 0.185       | 0.185       |
| $\nu(^{10}\text{He})$ (fm $^{-2}$ )                  |                     | 0.185       | 0.175       | 0.165       | 0.165       |
| exp.   |                     | v58         | v56         | m62         | m56         |
| $a_t$ (fm)   | 5.42 ( $p$ - $n$ )  | 9.7         | 5.4         | 6.4         | 4.2         |
| $a_s$ (fm)   | -16.5 ( $n$ - $n$ ) | 9.7         | -23.9       | 6.4         | >100        |
| $S_n(^5\text{He})$ (MeV)                             | -0.9                | -0.7        | -0.7        | -1.0        | -0.4        |
| $2E(^4\text{He}) - E(^4\text{He-}^4\text{He})$ (MeV) | -0.1                | 0.6         | 1.4         | -1.3        | -0.6        |
| $S_{2n}(^6\text{He})$ (MeV)                          | 1.0                 | 1.3         | -0.2        | 2.1         | 1.1         |
| $S_{2n}(^8\text{He})$ (MeV)                          | 2.1                 | 3.0         | 3.2         | 1.2         | 2.0         |

## B. Interactions

We used effective nuclear interaction consisting of the central force, the spin-orbit force and Coulomb force. As for the central force, we adopted the Volkov force[39] used in the work on He isotopes with AMD+GCM( $^4\text{He}+Xn$ )[20], and also the MV1 force[40] used in the AMD calculations of  $^{12}\text{C}$  [34, 42]. We used the spin-orbit force of the G3RS force[41] as done in [20, 42]. We fixed the strengths of the spin-orbit term as  $u_{ls} = 2000$  MeV, which is the same value as in [20]. By taking care of energies of subsystems, we tuned the interaction parameters,  $w$ ,  $b$ ,  $h$ ,  $m$ , for Wigner, Bartlett, Heisenberg and Majorana exchange terms in the central force(Volkov or MV1), respectively.  $^6\text{He}$ ,  $^8\text{He}$  and  $^{10}\text{He}$  were calculated with AMD+GCM by using totally 4 cases of central force. The parametrization for the central force is summarized in table I. In order to demonstrate characteristics of the effective interactions, we also show the relative energies of subsystems and the nucleon-nucleon scattering lengths with these 4 types of interaction. We estimate the energies of the  $^4\text{He}$ ,  $^4\text{He}-n$  state with  $J^\pi = 3/2^-$ , and  $^4\text{He}-^4\text{He}$  state with  $J^\pi = 0^+$ , by assuming the  $(0s)^4$  state of  $^4\text{He}$  and performing cluster-GCM calculations within the  $\alpha$ - $n$  and  $\alpha$ - $\alpha$  cluster models for simplicity.

The first case of interaction is Volkov No.2 force[39] with interaction parameters  $m = 0.58$ ,  $b = h = 0$ . This is the same effective interaction as that used in the AMD+GCM( $^4\text{He}+Xn$ ) by Itagaki et al. [20], which succeeded to systematically reproduce the binding energies of He isotopes. We note this interaction 'v58' in this paper. In spite of good agreement of the binding energies of He isotopes, the v58 force has a fault that 2 neutrons are bound in a free space. It is well known that the Volkov force with  $b = h = 0$  has too strong neutron-neutron attraction, because such the parametrization with no Bartlett term nor Heisenberg term gives the same interaction in the singlet-even channel as that in the triplet-even channel. In reality, the singlet-even channel has weaker attraction, and two neutrons are unbound. In order to describe dineutron correlation in neutron-rich nuclei it might be crucial to reproduce such the feature of two-nucleon system, though it does not matter in case of spin-isospin saturated systems like  $Z = N$  nuclei.

In the second case of interaction, we used Volkov No.2 force with modified interaction parameters as  $m = 0.56$ ,  $b = h = 0.15$ . This interaction (noted as 'v56') describes well the experimental  $S$ -wave scattering lengths of the  $n$ - $n$  and  $p$ - $n$  channels, and the unbound feature of 2-neutron system. The Majorana parameter  $m = 0.56$  was determined by adjusting the binding energy of  $^8\text{He}$  to the experimental data. However, this interaction fails to reproduce  $2n$  separation energies of  $^6\text{He}$  and  $^8\text{He}$ , and it also gives too strong attraction in  $^4\text{He}-^4\text{He}$  system.

The third interaction('m62') and the forth one('m56') listed in table I are based on the MV1 force[40]. The parametrization of the m62 interaction is  $m = 0.62$  and  $b = h = 0$ , which is the same as used in the AMD calculations of  $^{12}\text{C}$  [34, 42]. In case of the m62 interaction, two neutrons are bound in a free space as well as the Volkov force with  $b = h = 0$  like the v58 interaction. In the 'm56' interaction, we used the modified Bartlett and Heisenberg terms,  $b = h = 0.15$ , and the Majorana term  $m = 0.56$  which was adjusted to reproduce the binding energy of  $^8\text{He}$ . With the  $m = 0.56$  interaction, two neutrons are almost unbound in a free space, and other energies of subsystems are reasonably reproduced.

## C. Ground states of He isotopes

We show the calculated results of the ground states of He isotopes. The energies of He isotopes are shown in Fig. 1. The v58 and m56 interactions systematically reproduce the energies of  $^4\text{He}$ ,  $^6\text{He}$  and  $^8\text{He}$ , though they overestimate the  $^{10}\text{He}$  energy. On the other hand, the v56 and m62 interactions are poor in reproduction of the  $^6\text{He}$  energy, and therefore, they fail to reproduce two-neutron separation energies of  $^6\text{He}$  and  $^8\text{He}$  as shown in table I. Hereafter, we discuss the results obtained with the v58 and m56 interactions. We stress again that the v58 interaction well describes the energies of subsystems except for the fault of the too strong neutron-neutron interaction, while the m56 interaction reasonably reproduces the global features of the subsystem energies.

The calculated root-mean-square radii of proton, neutron and matter density are given in table II with the experimental data. The theoretical results of other calculations are also listed. Experimentally, extremely large radii of  $^6\text{He}$  and  $^8\text{He}$  have been reported by the reaction cross sections [25, 43, 44]. It has been suggested that the large radii originate in the remarkable enhancement of neutron radii due to the neutron-halo and neutron-skin structures in  $^6\text{He}$  and  $^8\text{He}$ , respectively. The empirical neutron radii are well described by the present calculations with the m56 interaction. On the other hand, the neutron radii calculated with the v58 interaction are slightly smaller than the empirical ones as well as the former AMD+GCM( $^4\text{He}+Xn$ ) calculations with the same v58 interaction[20]. The proton radii calculated with the m56 interaction are consistent with the observed data except for that of  $^4\text{He}$ . Figure 2 shows the proton density and neutron density. In  $^6\text{He}$ , the neutron density has a long tail at a large distance region. This is the neutron halo structure and is similar to the neutron density obtained by other calculations such as SVM[19]. In  $^8\text{He}$ , the neutron and proton density shows the neutron skin structure at the surface, which well corresponds to the discussion in [19, 25]. Thus, the present calculations with the m56 interaction systematically describe the ground-state properties of  $^6\text{He}$  and  $^8\text{He}$  such as energies and radii.

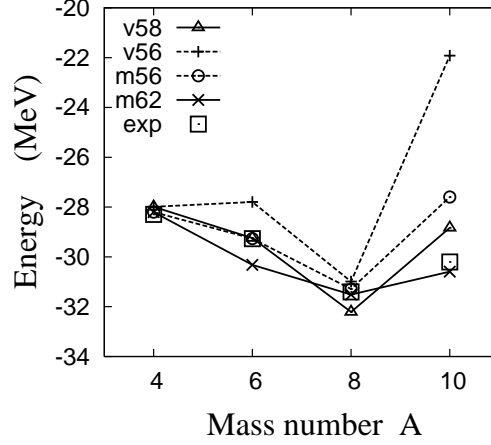


FIG. 1: The calculated energies of He isotopes with the v58, v56, m62 and m56 interactions(see text). The experimental data are also given.

Let us discuss the effect of the spin-orbit force, which may induce the  $j$ - $j$  coupling feature of neutrons. The expectation values of the spin-orbit force  $\langle V_{ls} \rangle$  and those of the squared total intrinsic spin of neutrons  $\langle S_n^2 \rangle$  are listed in table III. From the values of  $\langle S_n^2 \rangle$ , the  $S = 1$  component in the  ${}^6\text{He}(0_1^+)$  state is estimated to be 0.13 and 0.07 in the m56 and v58 results, respectively. It means that the  $(p_{3/2})^2$  configuration is contained due to the spin-orbit force. However, the  $S = 0$  component is still significant because of  $L$ - $S$  coupling feature of spin-zero  $2n$  correlation. We note that the fraction 0.87 in the m56 results for the  $S = 0$  component in  ${}^6\text{He}$  is in good agreement with three-body model calculations [7, 15, 16, 45]. Compared with the results of  ${}^6\text{He}$ , where the  $L$ - $S$  coupling configuration is significant as well as the  $j$ - $j$  coupling configuration, the  $j$ - $j$  coupling feature increases in the  ${}^8\text{He}(0_1^+)$  state because of the  $(p_{3/2})^4$  closure. As a result, the spin-orbit force gives much larger attraction in  ${}^8\text{He}$  by factor  $3 \sim 4$  than in  ${}^6\text{He}$ . It is interesting that the value  $\langle S_n^2 \rangle = 0.86(0.72)$  of the  ${}^8\text{He}(0_1^+)$  in the m56(v58) results is different from the value  $\langle S_n^2 \rangle = 1.33$  for the pure  $(p_{3/2})^4$  closed state. This deviation is because the  $L$ - $S$  coupling configuration is still contained in  ${}^8\text{He}$  due to the spin-zero  $2n$  correlation of neutron pairs. The detailed dineutron structure of  ${}^6\text{He}$  and  ${}^8\text{He}$  will be discussed later.

TABLE II: Root-mean-square radii (fm) of point-proton, point-neutron and point-matter density of the ground states of He isotopes. The experimental value(a) is deduced from the charge radius[46], and empirical values(b) are taken from [25, 44]. Theoretical values of other calculations, NCSM[10], SVM[19] AMD+GCM( ${}^4\text{He}+Xn$ )[20], RMF[14] are also given.

|                    | exp.  | AMD-v58                    | AMD-m56 | SVM[19] | RMF[14] | AMD( ${}^4\text{He}+Xn$ )[20] | NCSM[10] |
|--------------------|-------|----------------------------|---------|---------|---------|-------------------------------|----------|
| ${}^4\text{He}$    | $r_p$ | 1.455(1)                   | 1.46    | 1.64    |         |                               | 1.45     |
|                    | $r_n$ |                            | 1.46    | 1.64    |         |                               | 1.45     |
|                    | $r_m$ |                            | 1.46    | 1.64    | 1.76    |                               |          |
| ${}^6\text{He}$    | $r_p$ | 1.912(18) <sup>(a)</sup>   | 1.83    | 1.90    | 1.80    |                               | 1.89     |
|                    | $r_n$ | 2.59 – 2.61 <sup>(b)</sup> | 2.40    | 2.49    | 2.67    |                               | 2.67     |
|                    | $r_m$ | 2.33 – 2.48 <sup>(b)</sup> | 2.23    | 2.31    | 2.46    | 2.43                          | 2.32     |
| ${}^8\text{He}$    | $r_p$ | 1.76 – 2.15 <sup>(b)</sup> | 1.76    | 1.96    | 1.71    |                               | 1.88     |
|                    | $r_n$ | 2.64 – 2.69 <sup>(b)</sup> | 2.37    | 2.63    | 2.53    |                               | 2.8      |
|                    | $r_m$ | 2.49 – 2.52 <sup>(b)</sup> | 2.24    | 2.48    | 2.40    | 2.55                          | 2.31     |
| ${}^{10}\text{He}$ | $r_p$ |                            | 2.04    | 2.13    |         |                               |          |
|                    | $r_n$ |                            | 2.88    | 2.97    |         |                               |          |
|                    | $r_m$ |                            | 2.73    | 2.82    | 3.17    |                               |          |

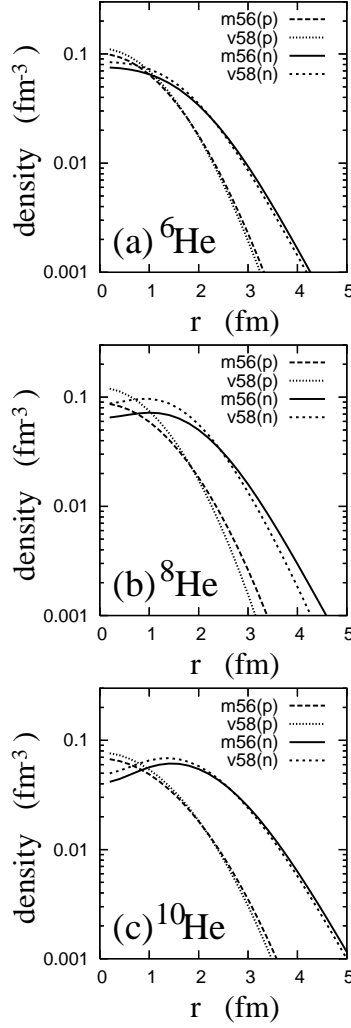


FIG. 2: Point-proton and point-neutron density in the ground states of He isotopes. The calculated results are those with the m56 and v58 interactions.

#### D. Excited states of $^8\text{He}$

The calculated energy levels of  $^8\text{He}$  are illustrated in Fig. 3, and the properties of the excited states are shown in table III. In both of the m56 and v58 results, the  $2_1^+$  state is the lowest excited state and the  $0_2^+$  state appears just above the  $2_1^+$  state. The  $1_1^-$  and  $3_1^-$  states are obtained in a higher energy region. In addition, in the present calculations with the m56 interaction, the  $1_1^+$ ,  $0_1^-$  and  $2_1^-$  states are obtained in almost the same energy region as the  $1_1^-$  and  $3_1^-$  states. The present AMD framework is regarded as a kind of bound state approximation because of the restricted model space, and therefore, coupling with continuum states is not taken into account. In such a case, only resonance states remain in low-energy region while continuum states rise to a high excitation energy region in principle. However, in order to check the stability of the resonances against neutron decays, their properties should be carefully examined. In the present m56 results, the negative-parity states contain large component of  $^6\text{He}+n+n$ -like configurations with the valence neutron far from the core. Since they have extremely large neutron radii and show somehow escaping behavior of neutrons, further investigation is required for these negative-parity states. In particular, the  $1_1^-$ ,  $2_1^-$  and  $0_1^-$  states can couple with  $(0s)^2(0p)^3(1s)^1$  neutron configuration which has a valence  $1s_{1/2}$  neutron with no centrifugal barrier.

Compared with the experimental data, the theoretical values of the  $2_1^+$  excitation energy are higher than the experimental one. However, it is important that the level structure for the excited states,  $2_1^+$ ,  $0_2^+$ ,  $1_1^-$  and  $3_1^-$ , is not sensitive to the adopted interaction though the relative position to the ground energy depends on the interaction.

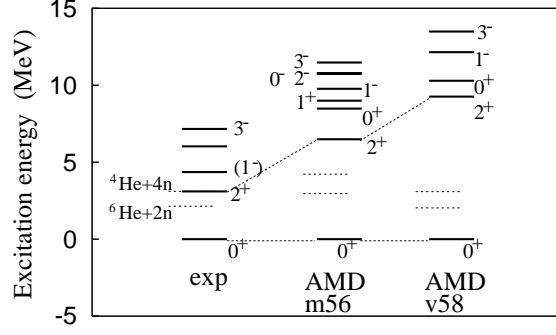


FIG. 3: Energy levels of  ${}^8\text{He}$ . The calculated results are those with the m56 and v58 interactions. The experimental data are taken from [47].

TABLE III: Excitation energies, Root-mean-square radii of point-proton, point-neutron and point-matter density, the expectation values of squared total intrinsic spin of neutrons  $\langle S_n^2 \rangle$ , and those of the spin-orbit force  $\langle V_{ls} \rangle$ .

| nucleus            | $J_n^\pi$ | exp.           | AMD-v58        |               |               |               |                         |                                   |  | AMD-m56        |               |               |               |                         |                                   |  |
|--------------------|-----------|----------------|----------------|---------------|---------------|---------------|-------------------------|-----------------------------------|--|----------------|---------------|---------------|---------------|-------------------------|-----------------------------------|--|
|                    |           | $E_x$<br>(MeV) | $E_x$<br>(MeV) | $r_p$<br>(fm) | $r_n$<br>(fm) | $r_m$<br>(fm) | $\langle S_n^2 \rangle$ | $\langle V_{ls} \rangle$<br>(MeV) |  | $E_x$<br>(MeV) | $r_p$<br>(fm) | $r_n$<br>(fm) | $r_m$<br>(fm) | $\langle S_n^2 \rangle$ | $\langle V_{ls} \rangle$<br>(MeV) |  |
| ${}^6\text{He}$    | $2_1^+$   | 1.797          | 3.2            | 1.82          | 2.42          | 2.23          | 0.19                    | -2.3                              |  | 2.6            | 1.87          | 2.46          | 2.28          | 0.27                    | -2.3                              |  |
| ${}^6\text{He}$    | $0_1^+$   | 0              | 0.0            | 1.83          | 2.40          | 2.23          | 0.16                    | -2.6                              |  | 0.0            | 1.90          | 2.49          | 2.31          | 0.26                    | -2.3                              |  |
| ${}^8\text{He}$    | $0_1^-$   |                |                |               |               |               |                         |                                   |  | 10.8           | 2.13          | 3.63          | 3.32          | 2.05                    | -5.9                              |  |
| ${}^8\text{He}$    | $2_1^-$   |                |                |               |               |               |                         |                                   |  | 10.8           | 2.07          | 3.41          | 3.13          | 2.00                    | -6.2                              |  |
| ${}^8\text{He}$    | $1_1^+$   |                |                |               |               |               |                         |                                   |  | 9.0            | 1.94          | 2.81          | 2.62          | 2.03                    | -2.5                              |  |
| ${}^8\text{He}$    | $3_1^-$   | 7.16           | 13.5           | 1.90          | 2.89          | 2.68          | 0.64                    | -6.7                              |  | 11.5           | 2.09          | 3.31          | 3.05          | 1.02                    | -5.3                              |  |
| ${}^8\text{He}$    | $1_1^-$   | 4.36           | 12.1           | 1.95          | 3.05          | 2.82          | 0.81                    | -7.9                              |  | 9.8            | 2.13          | 3.52          | 3.23          | 1.24                    | -5.8                              |  |
| ${}^8\text{He}$    | $0_2^+$   |                | 10.3           | 1.97          | 2.94          | 2.73          | 0.67                    | -4.7                              |  | 8.5            | 2.11          | 3.12          | 2.90          | 0.99                    | -1.0                              |  |
| ${}^8\text{He}$    | $2_1^+$   | 3.1            | 9.3            | 1.76          | 2.48          | 2.32          | 0.39                    | -4.8                              |  | 6.5            | 1.93          | 2.65          | 2.49          | 0.40                    | -2.8                              |  |
| ${}^8\text{He}$    | $0_1^+$   | 0              | 0.0            | 1.76          | 2.37          | 2.24          | 0.72                    | -11.4                             |  | 0.0            | 1.96          | 2.63          | 2.48          | 0.86                    | -7.3                              |  |
| ${}^{10}\text{He}$ | $0_1^+$   | 0              | 0.0            | 2.04          | 2.88          | 2.73          | 0.13                    | -2.6                              |  | 0.0            | 2.13          | 2.97          | 2.82          | 0.11                    | -1.7                              |  |

The  $0_2^+$  state is theoretically suggested to appear just above the  $2_1^+$  state. What is striking is that the  $0_2^+$  state has a remarkably large neutron radius compared with the ground state because of developed  ${}^4\text{He} + 2n + 2n$  structure. In the obtained wave function of the  $0_2^+$  state, which is given by a superposition of the basis AMD wave functions, the amplitude is found to be widely distributed into the basis wave functions with various spatial configuration of  ${}^4\text{He} + 2n + 2n$ . This indicates a gas-like feature that the dineutrons are rather freely moving around the  ${}^4\text{He}$  core. Therefore, we consider that the  $0_2^+$  state is the candidate of the cluster gas-like state with two dineutrons around the  $\alpha$  core. The detailed discussion of the dineutron-like structure is given later. In the experimental energy spectra, some excited states were observed above the  $2_1^+$  state. Spins and parities of these states are not definitely assigned yet. In the present calculations, the predicted  $0_2^+$  state has the strong monopole neutron transition from the ground states as the matrix element  $M_n(0_1^+ \rightarrow 0_2^+) = 13.5(13.9) \text{ fm}^2$  in the m56(v58) results. This neutron matrix element is much larger than the observed proton matrix element  $M_p(0_1^+ \rightarrow 0_2^+) = 5.4 \text{ fm}^2$  of  ${}^{12}\text{C}$  by more than factor 2. Therefore, we consider that the  ${}^8\text{He}(0_2^+)$  might be excited by inelastic scattering on nuclear target.

The excited states of  ${}^8\text{He}$  have been theoretically predicted by a few other calculations such as CSM and GFMC. The CSM gives better agreement of the  $2_1^+$  excitation energy with the experimental data[12]. We also comment that the GFMC calculation with AV18/IL2, which is an *ab initio* calculation with the realistic 2-body force and the empirical 3-body force, gives similar level structure to the present m56 results. Namely, the GFMC with AV18/IL2 gives the  $2^+$  state at  $E_x = 4.72 \text{ MeV}$  and the  $1_1^+$ ,  $0_2^+$  and  $2_2^+$  states in the  $E_x > 5 \text{ MeV}$  region.

## IV. DINEUTRON STRUCTURE

### A. What is dineutron( $^2n$ ) cluster ?

There is no bound state in an isolate  $nn$  system. However, it has been emphasized in many theoretical works that the spatial neutron-neutron correlation plays an important role in the binding mechanism of the Borromean systems with two-neutron halo such as  $^6\text{He}$  and  $^{11}\text{Li}$  (for example, [4, 5, 6, 48] and references therein). The neutron-neutron correlation is characterized by a spin-zero  $nn$  pair with spatial correlation in  $S$  wave. In the correlation density of two-neutron halo nuclei, a peak of the probability appears at the region with a small  $n$ - $n$  distance ( $R(nn)$ ) and a large  $n$ -core distance in general. This corresponds to the dineutron correlation. In an extended meaning, it is regarded as a “dineutron cluster” which can virtually exist in loosely bound neutron-rich nuclei.

As mentioned above, the characteristics of the dineutron are the zero spin and the spatial correlation. In the correlation density for  $^6\text{He}$ ,  $^{11}\text{Li}$  and  $^{14}\text{Be}$  given by three-body calculations [5, 7, 49, 50], the peak for the dineutron correlation are seen typically around the  $R(nn) \sim 2$  fm with a ridge in the  $R(nn) = 2 \sim 3$  fm region. It is important that this  $n$ - $n$  distance at the peak nearly depends on the system size among these three systems,  $^6\text{He}$ ,  $^{11}\text{Li}$  and  $^{14}\text{Be}$ . From this most probable  $n$ - $n$  distance, the typical size of the spatial correlation of the  $nn$  pair can be estimated to be about 2 fm. Then, we here approximately describe the dineutron cluster,  $^2n$ , by a spin-zero neutron pair written by the simple harmonic-oscillator  $(0s)^2$  state with the size parameter  $b$  in order to investigate dineutron structure in  $^8\text{He}$ . Then, the  $^2n$ -cluster wave function  $\phi^{^2n}(\mathbf{S})$  which is localized at the position  $\mathbf{S}$  is expressed as,

$$\phi^{^2n}(\mathbf{S}) = \mathcal{A} \{ \phi_{\mathbf{S}}^{0s}(\mathbf{r}_1) \chi_{\uparrow} \phi_{\mathbf{S}}^{0s}(\mathbf{r}_2) \chi_{\downarrow} \}, \quad (7)$$

$$\phi_{\mathbf{S}}^{0s}(\mathbf{r}_i) = \frac{1}{(b^2\pi)^{\frac{3}{4}}} \exp\left\{-\frac{1}{2b^2}(\mathbf{r}_i - \mathbf{S})^2\right\}. \quad (8)$$

In this definition, the relative motion between two neutrons in the  $^2n$  cluster is given by a Gaussian,

$$\phi^r(\mathbf{r}_1 - \mathbf{r}_2) = \frac{1}{(b_r^2\pi)^{\frac{3}{4}}} \exp\left\{-\frac{1}{2b_r^2}(\mathbf{r}_1 - \mathbf{r}_2)^2\right\}, \quad (9)$$

with the size  $b_r = \sqrt{2}b$ , which should be the typical  $nn$  distance  $b_r = 2 \sim 3$  fm. With this approximation of the  $^2n$  cluster, major component of the dineutron correlation might be taken into account, though the tail part at the large correlation length is omitted. For simplicity, we chose the size parameter  $b$  for the  $(0s)^2$  dineutron cluster as  $b = 1/\sqrt{2\nu}$ , where  $\nu$  is the width parameter  $\nu(^6\text{He})$  and  $\nu(^8\text{He})$  optimized for the  $^6\text{He}$  and  $^8\text{He}$ , respectively, in the AMD calculations. The values  $\nu$ , which are listed in table I, correspond to  $b_r = 2.0 - 2.3$  fm and satisfy the typical  $nn$  distance of the dineutron correlation.

### B. dineutron-cluster motion

In order to investigate features of dineutron cluster structure in the  $0^+$  states of  $^8\text{He}$ , we extracted the  $^2n$ -cluster motion from the obtained  $^8\text{He}(0^+)$  wave functions. We assume a simple core  $(^4\text{He} + ^2n)_{0^+}$  which is equivalent to the  $\text{SU}(3)$ -limit  $^6\text{He}(0^+)$ , and form the  $^6\text{He}^{SU(3)}(0^+)$ - $^2n$  cluster wave function with the  $L = 0$  relative motion between the core  $^6\text{He}^{SU(3)}(0^+)$  and the  $^2n$  cluster. In the same way as [34, 51] for  $\alpha$ -cluster motion, we calculated the reduced width amplitudes  $ry(r)$  for the  $^2n$ -cluster motion and the cluster probability  $S^{\text{fac}}$  by taking the overlap of the  $^6\text{He}^{SU(3)}(0^+)$ - $^2n$  cluster wave functions with the  $^8\text{He}$  wave functions. In Fig. 4, we show the reduced width amplitudes in the  $^8\text{He}(0_1^+)$  and the  $^8\text{He}(0_2^+)$  wave functions obtained by the v58 and m56 interactions. These indicate the  $^6\text{He}^{SU(3)}(0^+)$ - $^2n$  relative motion. We also show the reduced width amplitudes for the  $^8\text{Be}^{SU(3)}(0^+) - \alpha$  relative motion in the  $^{12}\text{C}(0_1^+)$  and  $^{12}\text{C}(0_2^+)$  given in [42]. Surprisingly, the  $^2n$ -cluster motion in the  $^8\text{He}$  is quite similar to the  $\alpha$ -cluster motion in the  $^{12}\text{C}$ .

First we discuss the features of the dineutron clustering in the  $0_2^+$  state. The most striking thing is that the  $^8\text{He}(0_2^+)$  state has the large amplitude of the dineutron cluster in the long distance region around  $r = 4 - 6$  fm, which well corresponds to the peak position of the  $\alpha$ -cluster motion in the  $^{12}\text{C}(0_2^+)$ . The enhancement of the  $^2n$ -cluster component at the long distance is more remarkable in the v58 results than the m56 results. The cluster probability of the  $^8\text{He}(0_2^+)$ , which is defined by the integrated overlap with the  $^6\text{He}^{SU(3)}(0^+)$ - $^2n$  cluster wave functions, is  $S^{\text{fac}} = 0.50$  and  $S^{\text{fac}} = 0.43$  in the v58 and the m56 results. The larger development of the  $^2n$  clustering in the v58 results is considered to be because of the stronger  $n$ - $n$  interaction in the v58 than the m56 interaction. It is very important that, even with the weaker  $n$ - $n$  interactions of the m56, the  $^2n$ -cluster structure survives with the significant component in the  $^8\text{He}(0_2^+)$ . Considering that the other  $^2n$  cluster exists inside the  $^6\text{He}^{SU(3)}(0^+)$  core, it is regarded that the



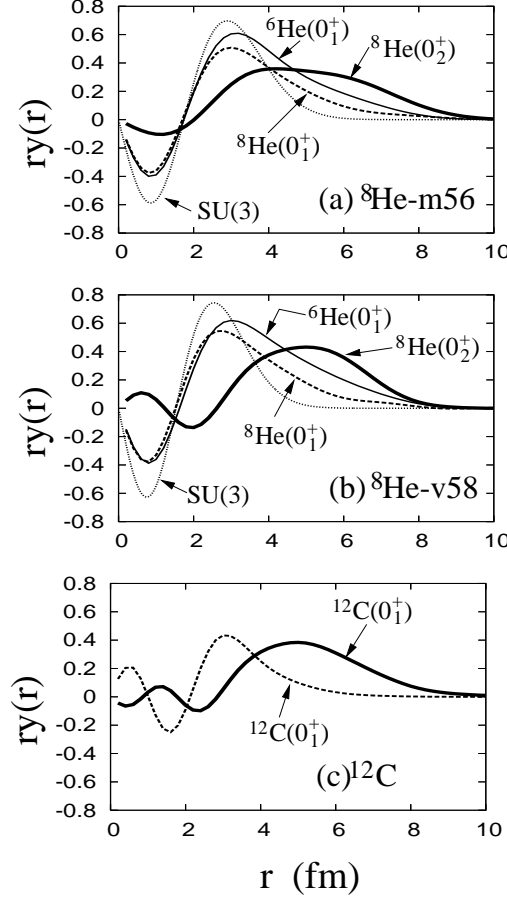


FIG. 4: Reduced width amplitudes  $ry_{l=0}(r)$  for  ${}^6\text{He}^{SU(3)}(0^+)-{}^2n$  in the  ${}^8\text{He}(0^+)$ , and those for  ${}^4\text{He}-{}^2n$  in the  ${}^6\text{He}(0^+)$ . The  ${}^8\text{He}(0^+)$  and  ${}^6\text{He}(0^+)$  wave functions are calculated by AMD+GCM with (a) the v58 and (b) the m56 interactions. The  ${}^6\text{He}^{SU(3)}(0^+)$  is written by a SU(3)-limit  ${}^4\text{He}-2n$  cluster state. The  ${}^4\text{He}$  cluster and the  ${}^2n$  cluster are expressed by the  $(0s)^4$  and  $(0s)^2$  wave functions, respectively, where the size parameter for the  $(0s)$  state is chosen to be the same value as the AMD+GCM wave functions;  $b = 1/\sqrt{2\nu({}^6\text{He})}$  in the calculation of  $ry(r)$  for  ${}^6\text{He}(0^+)$  and  $b = 1/\sqrt{2\nu({}^8\text{He})}$  in the calculation of  $ry(r)$  for  ${}^8\text{He}(0^+)$ . The reduced width amplitudes for  ${}^4\text{He}-{}^2n$  in the  ${}^6\text{He}^{SU(3)}(0^+)$  are also shown. (c) The reduced width amplitudes for  ${}^8\text{Be}^{SU(3)}(0^+)-\alpha$  in the  ${}^{12}\text{C}(0^+)$  taken from [34].

${}^8\text{He}(0_2^+)$  has the component of the developed  ${}^4\text{He}+{}^2n+{}^2n$  clustering, where two dineutrons are moving in  $L = 0$  orbits. Furthermore, from the analogy of the  ${}^2n$ -cluster structure in the  ${}^8\text{He}(0_2^+)$  with the  $\alpha$ -cluster structure in the  ${}^{12}\text{C}$ , the  ${}^8\text{He}(0_2^+)$  is considered to contain the dineutron gas-like structure.

Next, we discuss dineutron structure in the ground state of  ${}^8\text{He}$ . In the  ${}^8\text{He}(0_1^+)$ , the reduced width amplitude has a peak at the distance less than 3 fm. It means that the spatial development of the  ${}^2n$  cluster is not so remarkable as that of the  ${}^8\text{He}(0_2^+)$ . After discussing dineutron structure in the  ${}^6\text{He}(0_1^+)$ , we shall compare it with the dineutron structure in the  ${}^8\text{He}(0_1^+)$ . In Fig. 4, we show the reduced width amplitudes of the  ${}^4\text{He}-{}^2n$  cluster motion in the  ${}^6\text{He}(0_1^+)$  obtained by the present calculations, and that in the  ${}^6\text{He}^{SU(3)}(0^+)$  given by the SU(3)-limit  ${}^4\text{He}-{}^2n$  state. Compared with the SU(3)-limit, the calculated  ${}^6\text{He}(0_1^+)$  wave function has a long tail of dineutron structure at the surface. The  ${}^2n$ -cluster probability in the  ${}^6\text{He}(0_1^+)$  state is  $S^{\text{fac}} = 0.91$  and  $0.84$  in the v58 and the m56 calculations. This is consistent with the fraction,  $0.92$  and  $0.87$ , of the  $S = 0$  component, which are estimated from  $\langle S_n^2 \rangle$ . The  ${}^2n$ -cluster probability is reduced by the  $S = 1$  component because of the mixing of the  $(p_{3/2})^2$  state. The dineutron wave function in the inner region is similar to that of the SU(3)-limit  ${}^4\text{He}-{}^2n$  state. In this region, we have better to call it the spin-zero  $2n$  correlation(dineutron correlation) rather than the  ${}^2n$  cluster, because the antisymmetrization effect is important there.

Comparing the result of  ${}^8\text{He}(0_1^+)$  with that of  ${}^6\text{He}(0_1^+)$ , we found that the reduced width amplitude for the dineutron component is suppressed in the  ${}^8\text{He}(0_1^+)$ . This is because of the  $p_{3/2}$  sub-shell closure effect. As mentioned in the

previous section, the  $j$ - $j$  coupling feature is more remarkable in the  ${}^8\text{He}(0_1^+)$  than the  ${}^6\text{He}(0_1^+)$ . However, the cluster probability of the  ${}^8\text{He}(0_1^+)$  is still significant as  $S^{\text{fac}} = 0.57$  and  $0.52$  in the v58 and the m56 results, respectively. This probability dominantly originates in the SU(3)-limit  ${}^4\text{He}+{}^2n+{}^2n$  configuration, which is equivalent to the  $L$ - $S$  coupling  $p$ -shell configuration. It means that the dineutron correlation is still important in the  ${}^8\text{He}(0_1^+)$ . This situation is quite similar to that of the  ${}^{12}\text{C}(0_1^+)$  which is the admixture of the  $p_{3/2}$  closure and the SU(3)-limit  $3\alpha$  state. As a result of the  $L$ - $S$  coupling feature due to the dineutron correlation, the  ${}^8\text{He}(0_1^+)$  state should contain the significant  $(p_{3/2})^2(p_{1/2})^2$  contamination. This result is consistent with the experimental indication of the  $p_{1/2}$  component in the  ${}^8\text{He}$  ground state reported by the recent observations[27, 28]. As seen in Fig. 4, it is also interesting that the  ${}^8\text{He}(0_1^+)$  state has a tail of the  ${}^2n$ -cluster motion at the surface, though the tail is slight compared with the long tail in the  ${}^6\text{He}(0_1^+)$ . In conclusion, the  ${}^8\text{He}(0_1^+)$  is the admixture of the  $p_{3/2}$  closure and the  $L$ - $S$  coupling  $p$ -shell configuration of neutrons with a small tail of the dineutron clustering.

### C. ${}^2n$ condensate wave function

In the previous subsection, we discuss the  ${}^2n$ -cluster wave function by assuming the core  $({}^4\text{He}+{}^2n)_{0+}$  which is equivalent to the SU(3)-limit  ${}^6\text{He}(0^+)$ . In this description, one of the  ${}^2n$  clusters is confined in the the core  $({}^4\text{He}+{}^2n)_{0+}$ , and its relative wave function to the  ${}^4\text{He}$  is given by the  $1s$  orbit of the harmonic oscillator potential with the oscillator frequency  $\omega = 8\nu/3$ .

As shown in Fig. 4, in this SU(3)-limit, the radial wave function of the  ${}^2n$ -cluster around the  ${}^4\text{He}$  remains in the inner region. In such the case, although the  ${}^2n$ -cluster is moving in the  $S$  wave, the  ${}^2n$ -cluster receives much effect of antisymmetrization from the  ${}^4\text{He}$  core and it does not necessarily indicate a gas-like state. In order to see more directly the  ${}^2n$ -cluster gas-like nature, where two  ${}^2n$ 's are moving in  $S$  wave far from the the  ${}^4\text{He}$  core, we assumed the  ${}^2n$  condensate wave function in the  ${}^4\text{He}+{}^2n+{}^2n$  system and calculated the overlap with the obtained  ${}^8\text{He}(0^+)$  wave functions.

We define the  ${}^2n$  condensate wave function by naturally extending the  $\alpha$  condensate wave function proposed by Tohsaki et al.[1] as follows,

$$\Psi_{\text{cond}}(B) \equiv n_0 \int \prod_{i=1}^k \left\{ d^3\mathbf{S}_i \exp \left( -\frac{(\mathbf{S}_i - \mathbf{S}_C)^2}{B^2} \right) \right\} \Phi_{\text{Brink}}(\mathbf{S}_C, \mathbf{S}_1, \mathbf{S}_2, \dots, \mathbf{S}_k), \quad (10)$$

where  $n_0$  is the normalization factor and  $\Phi_{\text{Brink}}(\mathbf{S}_C, \mathbf{S}_1, \mathbf{S}_2, \dots, \mathbf{S}_k)$  is the Brink wave function for the  $C+k({}^2n)$ -cluster system consisting the core( $C$ ) and  $k$  dineutrons( ${}^2n$ ) as,

$$\Phi_{\text{Brink}}(\mathbf{S}_C, \mathbf{S}_1, \mathbf{S}_2, \dots, \mathbf{S}_k) \equiv \mathcal{A} \left\{ \phi^C(\mathbf{S}_C) \phi^{2n}(\mathbf{S}_1) \phi^{2n}(\mathbf{S}_2) \dots \phi^{2n}(\mathbf{S}_k) \right\}. \quad (11)$$

Here, the wave function of the  $i$ th  ${}^2n$ ,  $\phi^{2n}(\mathbf{S}_i)$ , is given by the  $(0s)^2$  state localized around  $\mathbf{S}_i$ .  $\mathbf{S}_C$  is the mean position of the center of mass motion of the core, and is chosen to be  $\mathbf{S}_C = -\frac{2}{A}(\mathbf{S}_1 + \mathbf{S}_2 + \dots + \mathbf{S}_k)$ . In heavy limit of the core mass  $A$ , this wave function is equivalent to the dineutron condensate wave function proposed by Horiuchi[52]. In the present calculation for  ${}^4\text{He}+{}^2n+{}^2n$ , the core  $C$  is  ${}^4\text{He}$ , and the number of  ${}^2n$  clusters is  $k = 2$ . We assumed the  $(0s)^4$  state of the core wave function,  $\phi^{4\text{He}}$ , and adopted the common size parameter  $b = 1/\sqrt{(2\nu({}^8\text{He}))}$  for the  ${}^4\text{He}$  and  ${}^2n$  clusters. In the practical calculations, the 6-dimensional integrals for the coordinates,  $\mathbf{S}_1$  and  $\mathbf{S}_2$ , are performed by taking mesh points on  $(\theta_{12}, |\mathbf{S}_1|, |\mathbf{S}_2|)$  and the total-angular-momentum projection ( $\theta_{12}$  is the angle between  $\mathbf{S}_1$  and  $\mathbf{S}_2$ ).

In Fig. 5, we show the squared overlap,  $|\langle {}^8\text{He} | \Psi_{\text{cond}}(B) \rangle|^2$ , between the  ${}^2n$  condensate wave function and the  ${}^8\text{He}$  wave functions obtained by AMD+GCM. The calculated values are plotted as a function  $B$  which indicates the size of the spatial distribution of  ${}^2n$  clusters in the condensate wave function. The  ${}^8\text{He}(0_1^+)$  has the overlap, about 0.5, at  $B < 2$  fm. The condensate wave function  $\Psi_{\text{cond}}(B)$  with such a small size  $B$  is almost equivalent to the SU(3)-limit  ${}^4\text{He}+{}^2n+{}^2n$  state. On the other hand, the  ${}^8\text{He}(0_2^+)$  has the maximum overlap, about 0.5, at remarkably large size  $B = 4 - 5$  fm. This is a strong indication of the dineutron gas-like component in the calculated  ${}^8\text{He}(0_2^+)$ . The dineutron gas-like feature is further enhanced in case of the v58 interaction than the m56 interaction. These results are consistent with the discussion of the  ${}^2n$ -cluster wave function in the previous subsection.

## V. SUMMARY

We studied the structure of  ${}^8\text{He}$  with a method of AMD+GCM. We chose the effective nuclear interactions by taking care of energies of subsystems, and reproduced the properties of ground states of  ${}^4\text{He}$ ,  ${}^6\text{He}$  and  ${}^8\text{He}$ . In the

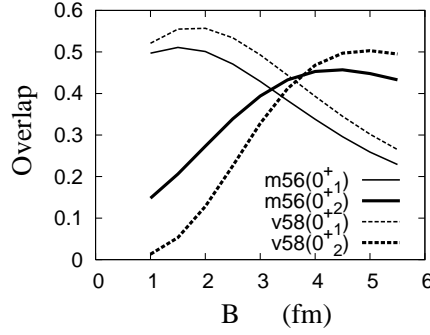


FIG. 5: The squared overlap between the dineutron condensate wave function  $\Psi_{\text{cond}}(B)$  and the obtained  ${}^8\text{He}(0^+)$  wave functions. See details in the text.

ground state of  ${}^8\text{He}$ , the component of the  $p_{3/2}$  sub-shell closure is dominant. However, the  $L$ - $S$  coupling feature is also significantly contained because of the spin-zero dineutron correlation. This is consistent with the experimental report on the significant mixing of  $(p_{3/2})^2(p_{1/2})^2$  component in the  ${}^8\text{He}(0_1^+)$ . It is concluded that the  ${}^8\text{He}(0_1^+)$  is the admixture of  $p_{3/2}$  sub-shell closure and  $L$ - $S$  coupling  $p$ -shell configurations with a slight dineutron tail at the surface. This result is also consistent with the experimentally suggested large spectroscopic factor of the  ${}^6\text{He}(2^+)$  in the  ${}^8\text{He}(0_1^+)$ .

The present results suggest that the  $0_2^+$  state may appear a few MeV above the  $2_1^+$  state. By analyzing dineutron structure, it was found that this state has a significant component of the developed  ${}^4\text{He}+{}^2n+{}^2n$  structure where two dineutrons are moving around the  ${}^4\text{He}$  core in  $S$  wave with a dilute density. The  ${}^2n$ -cluster wave function of the  ${}^8\text{He}(0_2^+)$  state is similar to the  $\alpha$ -cluster wave function of the  ${}^{12}\text{C}(0_2^+)$  state. Therefore, we consider that the predicted  $0_2^+$  state is the candidate of the dineutron gas-like state, which is analogy to the  $\alpha$  condensate state suggested in the  ${}^{12}\text{C}(0_2^+)$ . In the experimental energy spectra of  ${}^8\text{He}$ , some excited states were observed above the  $2_1^+$  state. Spins and parities of these states have not been definitely assigned yet. Since the present calculations predicted the remarkable neutron matrix element for the monopole transitions  ${}^8\text{He}(0_1^+) \rightarrow {}^8\text{He}(0_2^+)$ , we expect that the  ${}^8\text{He}(0_2^+)$  might be excited in inelastic scattering on nuclear target.

Since the AMD framework is regarded as a kind of bound state approximation because of the restricted model space, coupling with continuum states is not taken into account. In future study, widths of the excited states should be carefully investigated by taking into account the continuum coupling in order to confirm the stability of the resonances against particle decays.

In the present work, the calculations were performed within the AMD model space by using effective interactions. We chose the interaction parameters by taking care of subsystem energies such as  $\alpha$ - $n$ ,  ${}^6\text{He}$  as well as nucleon-nucleon systems. Although it is difficult to completely reproduce all of the subsystem energies with a unique effective interaction, we found the interaction which can reasonably reproduce the global feature of the subsystem energies. We here stress that the level structure of the excited states is not sensitive to the adopted nuclear forces within the reasonable choice of effective interaction, though the excitation energy relative to the ground state depends on the interaction. It is also important that the dineutron structure of the  ${}^8\text{He}(0^+)$  states is qualitatively similar among four sets of interaction adopted in the present calculations. For further investigations of He isotopes, more extended calculations based on the realistic forces should be important as well as *ab initio* calculations.

### Acknowledgments

The authors would like to thank Prof. Horiuchi, Prof. Tohsaki and their collaborators for valuable discussions. They are also thankful to members of Yukawa Institute for Theoretical Physics(YITP) and Department of Physics in Kyoto University, especially Dr. Takashina for fruitful discussions. The computational calculations in this work were performed by the Supercomputer Projects of High Energy Accelerator Research Organization(KEK) and also the super computers of YITP. This work was supported by Grant-in-Aid for Scientific Research Japan Society for the Promotion of Science and a Grant-in-Aid for Scientific Research from JSPS. It is also supported by the Grant-in-Aid for the 21st Century COE "Center for Diversity and Universality in Physics" from MEXT. Discussions in the RCNP workshops on cluster physics held in 2007 and those in the workshops YITP-W-06-17 and YITP-W-07-01 held in

YITP were helpful to initiate and complete this work.

- 
- [1] A. Tohsaki, H. Horiuchi, P. Schuck, and G. Röpke, Phys. Rev. Lett. **87**, 192501 (2001).
  - [2] G. Röpke, A. Schnell, P. Schuck, and P. Nozieres, Phys. Rev. Lett. **80**, 3177 (1998).
  - [3] M. Matsuo, Phys. Rev. C **73**, 044309 (2006).
  - [4] G. F. Bertsch and H. Esbensen, Ann. Phys. (NY) **209**, 327 (1991).
  - [5] M. V. Zhukov *et al.*, Phys. Rep. **231**, 151 (1993).
  - [6] S. Aoyama, K. Kato, and K. Ikeda, Prog. Theor. Phys. Suppl. **142**, 35 (2001).
  - [7] K. Arai, Y. Ogawa, Y. Suzuki, and K. Varga, Prog. Theor. Phys. Suppl. **142**, 97 (2001).
  - [8] S. C. Pieper, R. B. Wiringa, and J. Carlson, Phys. Rev. C **70**, 054325 (2004).
  - [9] S. C. Pieper, Nucl. Phys. A **751**, 516c (2005).
  - [10] E. Caurier and P. Navrátil, Phys. Rev. C **73**, 021302(R) (2006).
  - [11] N. Michel, W. Nazarewicz, M. Płoszajczak, and J. Okolowicz Phys. Rev. C **67**, 054311 (2003).
  - [12] A. Volya and V. Zelevinsky, Phys. Rev. Lett. **94**, 052501 (2005); A. Volya and V. Zelevinsky, Phys. Rev. C **74**, 064314 (2006).
  - [13] G. Hagen, M. Hjorth-Jensen, and J. S. Vaagen, Phys. Rev. C **71**, 044314 (2005).
  - [14] Y. Sugahara *et al.*, Prog. Theor. Phys. **96** 1165 (1996).
  - [15] A. Csötö, Phys. Rev. C **48**, 165 (1993).
  - [16] D. Baye, M. Kruglanski and M. Vincke, Nucl. Phys. A **573**, 431 (1994).
  - [17] S. Aoyama, Phys. Rev. Lett. **89**, 052501 (2002).
  - [18] Y. Suzuki, and W. J. Ju, Phys. Rev. C **41** 736 (1990).
  - [19] K. Varga, Y. Suzuki, and Y. Ohbayasi, Phys. Rev. C **50**, 189 (1994).
  - [20] N. Itagaki and S. Aoyama, Phys. Rev. C **61**, 024303 (2000).
  - [21] H. Masui, K. Katō, and K. Ikeda, Phys. Rev. C **75**, 034316(2007).
  - [22] A. Doté and H. Horiuchi, Prog. Theor. Phys. **103**, 261 (2000).
  - [23] S. Aoyama, N. Itagaki, and M. Oi, Phys. Rev. C **74**, 017307 (2006).
  - [24] T. Neff, H. Feldmeier, and R. Roth, Nucl. Phys. A **752**, 321c (2005).
  - [25] I. Tanihata *et al.*, Phys. Lett. **289B**, 261 (1992).
  - [26] A. A. Korshennikov *et al.* Phys. Rev. Lett. **90**, 082501 (2003).
  - [27] L. V. Chulkov *et al.*, Nucl. Phys. A **759** 43 (2005).
  - [28] N. Keeley *et al.*, Phys. Lett. **B646**, 222 (2007).
  - [29] F. Skaza *et al.*, Phys. Rev. C **73**, 044301 (2006).
  - [30] A. A. Korshennikov *et al.*, Phys. Lett. **B 316**, 38 (1993).
  - [31] Y. Kanada-En'yo, H. Horiuchi and A. Ono, Phys. Rev. C **52**, 628 (1995); Y. Kanada-En'yo and H. Horiuchi, Phys. Rev. C **52**, 647 (1995).
  - [32] Y. Kanada-En'yo and H. Horiuchi, Prog. Theor. Phys. Suppl. **142**, 205 (2001).
  - [33] Y. Kanada-En'yo, M. Kimura and H. Horiuchi, Comptes rendus Physique Vol.4, 497 (2003).
  - [34] Y. Kanada-En'yo, Prog. Theor. Phys. **117**, 655 (2007).
  - [35] Y. Kanada-En'yo, Phys. Rev. C **75**, 024302 (2007).
  - [36] M. Kimura and H. Horiuchi, Prog. Theor. Phys. **111**, 841 (2004).
  - [37] Y. Kanada-En'yo and Y. Akaishi, Phys. Rev. C **69**, 034306 (2004).
  - [38] A. Dote, H. Horiuchi, and Y. Kanada-En'yo, Phys. Rev. C **56**, 1844 (1997).
  - [39] A. B. Volkov, Nucl. Phys. **74**, 33 (1965).
  - [40] T. Ando, K. Ikeda and A. Tohsaki, Prog. Theor. Phys. **64**, 1608 (1980).
  - [41] N. Yamaguchi, T. Kasahara, S. Nagata and Y. Akaishi, Prog. Theor. Phys. **62**, 1018 (1979); R. Tamagaki, Prog. Theor. Phys. **39**, 91 (1968).
  - [42] Y. Kanada-En'yo, Phys. Rev. Lett. **81**, 5291 (1998).
  - [43] I. Tanihata *et al.*, Phys. Rev. Lett. **55**, 2676 (1985).
  - [44] I. Tanihata *et al.*, Phys. Lett. B **206**, 592 (1988).
  - [45] K. Hagino and H. Sagawa, Phys. Rev. C **72**, 044321 (2005).
  - [46] L. -B. Wang *et al.* Phys. Rev. Lett. **93**, 142501 (2004).
  - [47] D. R. Tilley *et al.*, Nucl. Phys. A **745**, 155 (2004).
  - [48] S. Aoyama, A. Muraki, K. Katō, and K. Ikeda, Prog. Theor. Phys. **93**, 99 (1995).
  - [49] P. Descouvemont, C. Daniel, and D. Baye, Phys. Rev. C **67**, 044309 (2003).
  - [50] P. Descouvemont, E. Tursunov, and D. Baye, Nucl. Phys. A **765**, 370 (2006).
  - [51] Y. Kanada-En'yo and H. Horiuchi, Phys. Rev. C **68**, 014319 (2003).
  - [52] H. Horiuchi, Mod. Phys. Lett. **A21**, Nos.31-33, 2455 (2006).